Theoretical Study of $HCN^+ + C_2H_2$ Reaction

Yan Li, Hui-ling Liu, Xu-ri Huang,* De-quan Wang, Chia-chung Sun, and Au-chin Tang

State Key Laboratory of Theoretical and Computational Chemistry, Institute of Theoretical Chemistry, Jilin University, Changchun 130023, People's Republic of China

Received: February 15, 2008; Revised Manuscript Received: May 28, 2008

A detailed theoretical investigation for the ion−molecule reaction of HCN^+ with C_2H_2 is performed at the B3LYP/6-311G(d,p) and CCSD(T)/6-311++G(3df,2pd) (single-point) levels. Possible energetically allowed reaction pathways leading to various low-lying dissociation products are probed. It is shown that eight dissociation products $\mathbf{P_1}$($H_2C_3N^+$+H), $\mathbf{P_2}$(CN+$C_2H_3^+$), $\mathbf{P_3}$(HC_3N^++H_2), $\mathbf{P_4}$ ($HCCCNH^+$+H), $\mathbf{P_5}$(H_2NCCC^++H), $\mathbf{P_6}$($HCNCCH^+$+H), $\mathbf{P_7}$($C_2H_2^+$+HCN), and $\mathbf{P_8}$ ($C_2H_2^+$+HNC) are both thermodynamically and kinetically accessible. Among the eight dissociation products, $\mathbf{P_1}$ is the most abundant product. $\mathbf{P_7}$ and $\mathbf{P_3}$ are the second and third feasible products but much less competitive than $\mathbf{P_1}$, followed by the almost negligible product $\mathbf{P_2}$. Other products, $\mathbf{P_4}$ ($HCCCNH^+$+H), $\mathbf{P_5}$ ($HCNCCH^+$+H), $\mathbf{P_6}$ (H_2NCCC^++H), and $\mathbf{P_8}$ ($C_2H_2^+$+HNC) may become feasible at high temperatures. Because the intermediates and transition states involved in the reaction $HCN^+ + C_2H_2$ are all lower than the reactant in energy, the title reaction is expected to be rapid, as is consistent with the measured large rate constant at room temperature. The present calculation results may provide a useful guide for understanding the mechanism of HCN^+ toward other π-bonded molecules.

1. Introduction

Titan, the largest satellite of Saturn, is of considerable interest since its atmosphere is so various and it is one of the places where the most complex atmosphere organic chemistry takes place in the solar system. A number of investigations have been carried out to provide an understanding of the structure and composition of this atmosphere.[1–4] It has been established that Titan's atmosphere consists mainly of nitrogen gas and with traces of numerous hydrocarbons.[5–7] Species such as hydrogen cyanide (HCN), methyl cyanide (CH_3CN), cyanoacetylene (HC_3N), and cyanogen (C_2N_2) are also present in much lower abundance.[8,9] Neutral species are ionized by a combination of photoionization by solar radiations and electron impact ionization by Saturn's magnetospheric electrons.[10,11] Then the primary ions N^+ and N_2^+ react with methane (CH_4) to produce CH_2^+, CH_3^+, CH_4^+, and HCN^+. Subsequently, these ions react further with the hydrocarbons that are present in Titan's atmosphere such as methane (CH_4), acetylene (C_2H_2), ethylene (C_2H_4), ethane (C_2H_6), and so on. In this way, a complex matrix of reactions is quickly established. Such reactions are generally very fast and may be very effective in depleting old molecules or ions and synthesizing new molecules or ions.

Acetylene (C_2H_2) is an archetype of C≡C triple bonding for hydrocarbons, and it plays a crucial role in various fields, such as combustion chemistry, photochemistry, organic chemistry, catalytic reactions, and so forth. Up to now, a large number of experimental and theoretical investigations have been performed on the neutral-C_2H_2 reactions, such as NCO,[12] F/Cl,[13] CP,[14] HCO/HOC,[15] HCCCO,[16] NCX (X = O, S),[17] and CN.[18] Also, there have been numerous studies on the ion-C_2H_2 reactions such as HCN^+,[19] $HCNH^+$,[20] CH^+,[21] O^-,[22] S^+,[23] HCO^+,[24] $HCCCH_2^+$,[25] CH_2F^+,[26] O^+,[27] O_2^+,[28] and CH_3CHO^+.[29] Among the C_2H_2 reactions, the reaction with HCN^+ attracts our greatest interest. According to the experimental studies that were performed by Anicich et al. at room temperature using the following after low-selected ion flow tube (FA-SIFT), the products and distributions are as follows

$$HCN^+ + C_2H_2 \rightarrow C_2H_2^+ + HCN \quad 0.19$$
$$\rightarrow C_2H_3^+ + CN \quad 0.01$$
$$\rightarrow C_3N^+ + H_2 + H \quad 0.06$$
$$\rightarrow HC_3N^+ + H_2 \quad 0.09$$
$$\rightarrow H_2C_3N^+ + H \quad 0.66$$

But to the best of our knowledge, there is no theoretical study on this reaction up to now. In the present paper, we investigate a detailed theoretical study on the reaction mechanism of HCN^+ with C_2H_2.

2. Computational Methods

All calculations are performed with the Gaussian 98 program package.[30] The geometries of reactant, products, intermediates, and transition states are initially optimized at the density functional theory (DFT) B3LYP[31] with 6-311G(d,p) basis set. Frequency calculations are performed at the same level to check the obtained species is an isomer (with all real frequencies) or a transition state (with one and only one imaginary frequency). Intrinsic reaction coordinate (IRC)[32] calculations are performed at the B3LYP/6-311G(d,p) level to confirm that the transition state connects the designated intermediates. To obtain more reliable energetic data, single-point energy calculations are carried out at the CCSD(T)/6-311++G(3df,2pd)[33] level using the B3LYP/6-311G(d,p) optimized geometries.

* To whom correspondence should be addressed.

10.1021/jp801352z CCC: $40.75 © 2008 American Chemical Society
Published on Web 08/12/2008

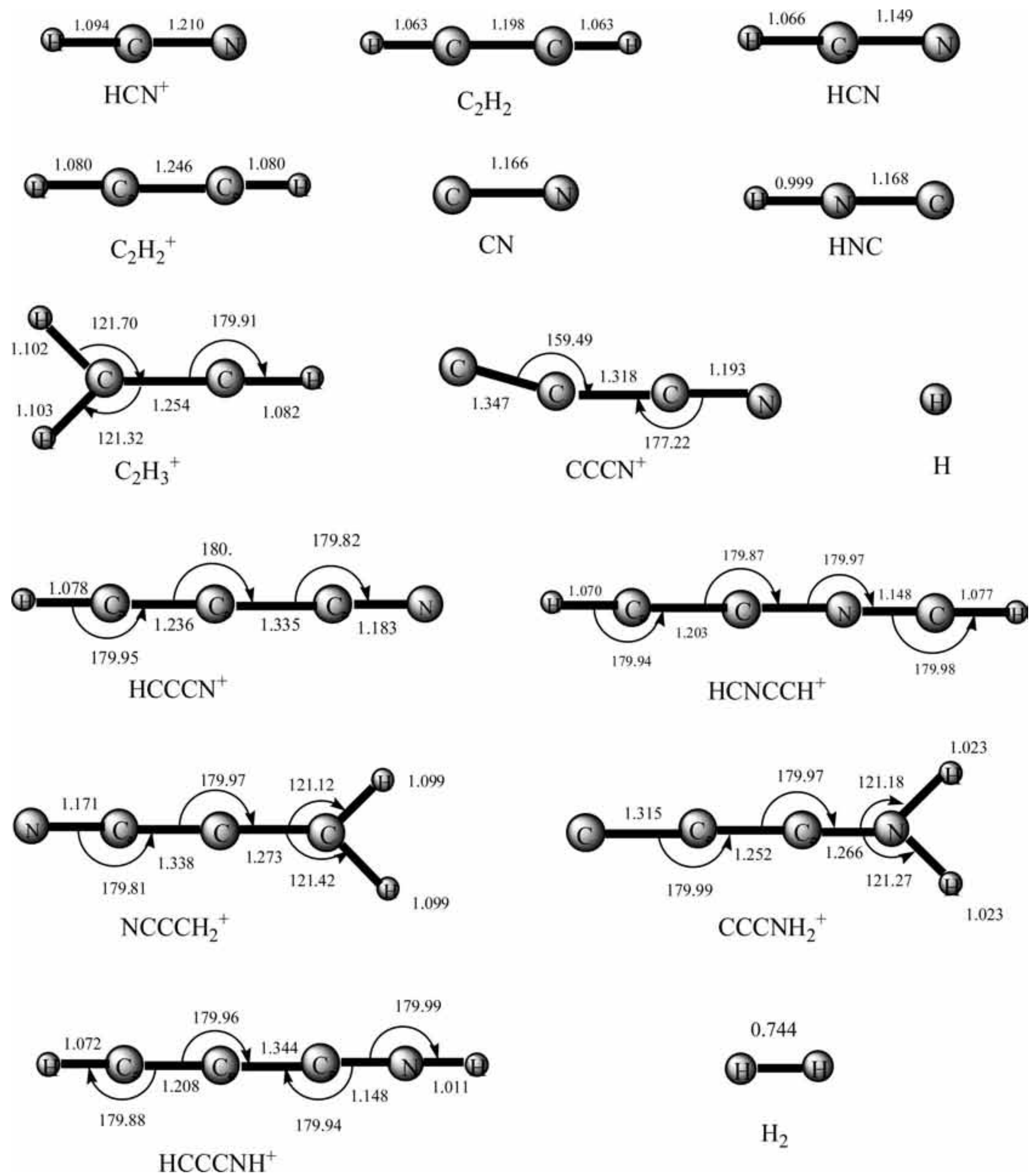

Figure 1. The optimized structures of the reactant, products. Distances are given in angstroms and angles in degrees.

3. Results and Discussion

The optimized structures of reactant and products are shown in Figure 1, and the optimized structures of intermediates and transition states are shown in Figures 2 and 3, respectively. The symbol **TSm/n** is used to denote the transition state connecting isomers **m** and **n**. The total and relative energies are listed in Table 1 for reactant and products, while in Table 2 for intermediates and transition states. By means of reactant, intermediates, transition states and products, a schematic potential energy surface (PES) for the reaction of $HCN^+ + C_2H_2$ is plotted in Figure 4. Unless otherwise specified, the relative energies at CCSD(T)/6-311++G(3df,2pd)//B3LYP/6-311G(d,p)+ZPVE (zero-point vibrational energy) level are used in the following discussion. Furthermore, for understanding the reaction mechanism easily, we shown a simple frame graph in Scheme 1. It should be pointed out that the value behind every species is its relative energy with respect to reactant, and the value on every arrowhead is the activation energy.

3.1. Entrance Channels. The attack of HCN^+ on the C_2H_2 molecule may have two kinds of entrance pathways: (i) C addition to form **1** (*p*-$HCCHCHN^+$) and **2** (*υ*-$HCCHCHN^+$) without any encounter barriers (as shown in Figure 4a), (◆)N addition to form **3** ($HCNCHCH^+$) (as shown in Figure 4b). Although the low-lying intermediate **3** ($HCNCHCH^+$) has two isomeric forms, **3a** and **3b**, we are unable to find the transition state connecting them despite numerous attempts. As can be seen in Figure 2, the calculated CC bond length in **3a** and **3b** is 1.314 and 1.312 Å, respectively, and they are typical C═C double bond. Even if there is a transition state, a considerable rotary energy barrier should be overcome. In addition, we obtain a three-memberd ring isomer **12** (c-HCCHN-CH^+) which can be considered to form via the direct attack of N at the CC double bond of C_2H_2. But the only reaction channel from **12** is an evolution which isomerizes to **3b** as shown in Figure 4b.

The feasible N-addition and C-addition attacks can find support from spin distribution analysis. The spin densities on C and N are 0.419427e and 0.594288e, respectively, at the B3LYP/6-311G(d,p)

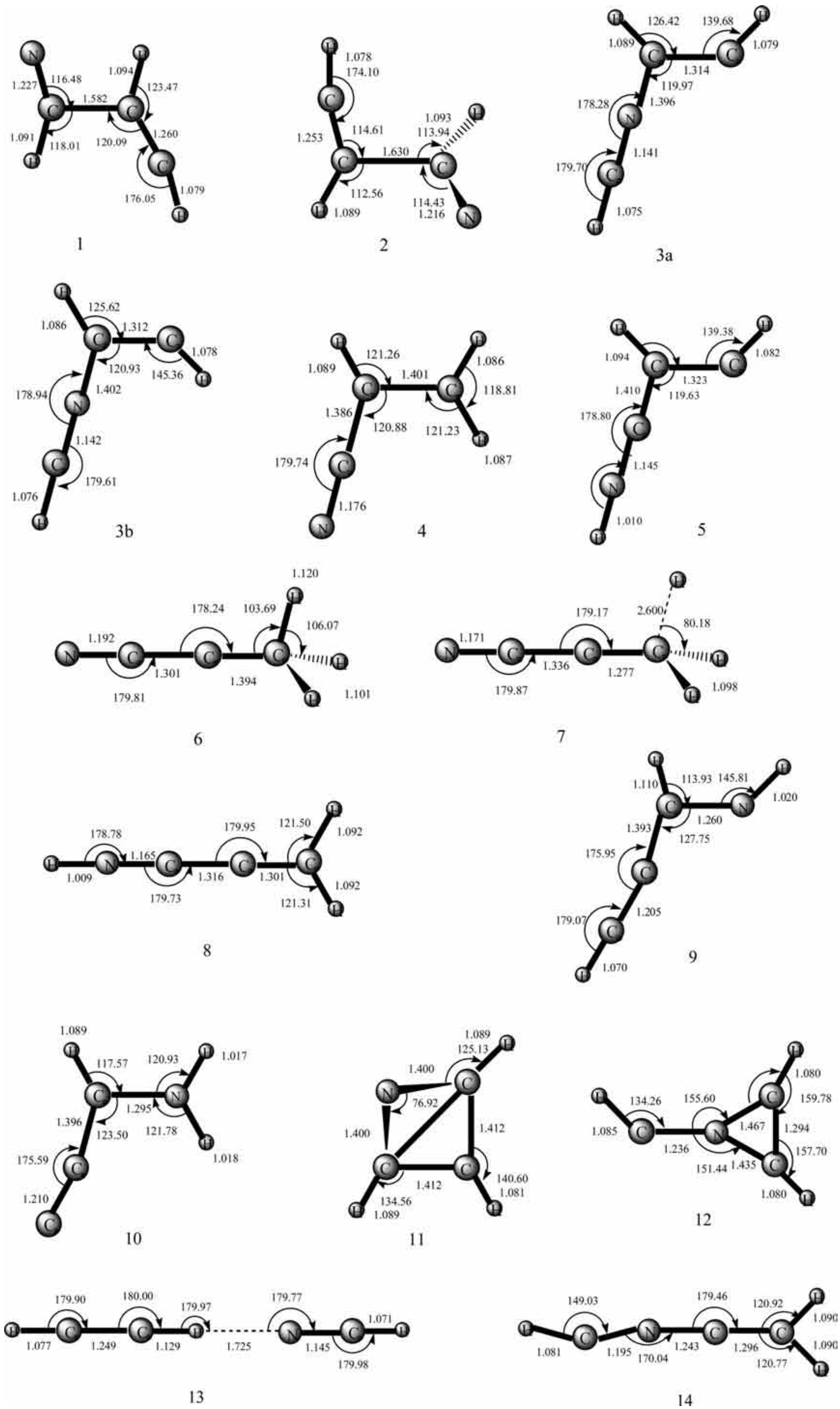

Figure 2. The optimized structures of the intermediates. Distances are given in angstroms and angles in degrees.

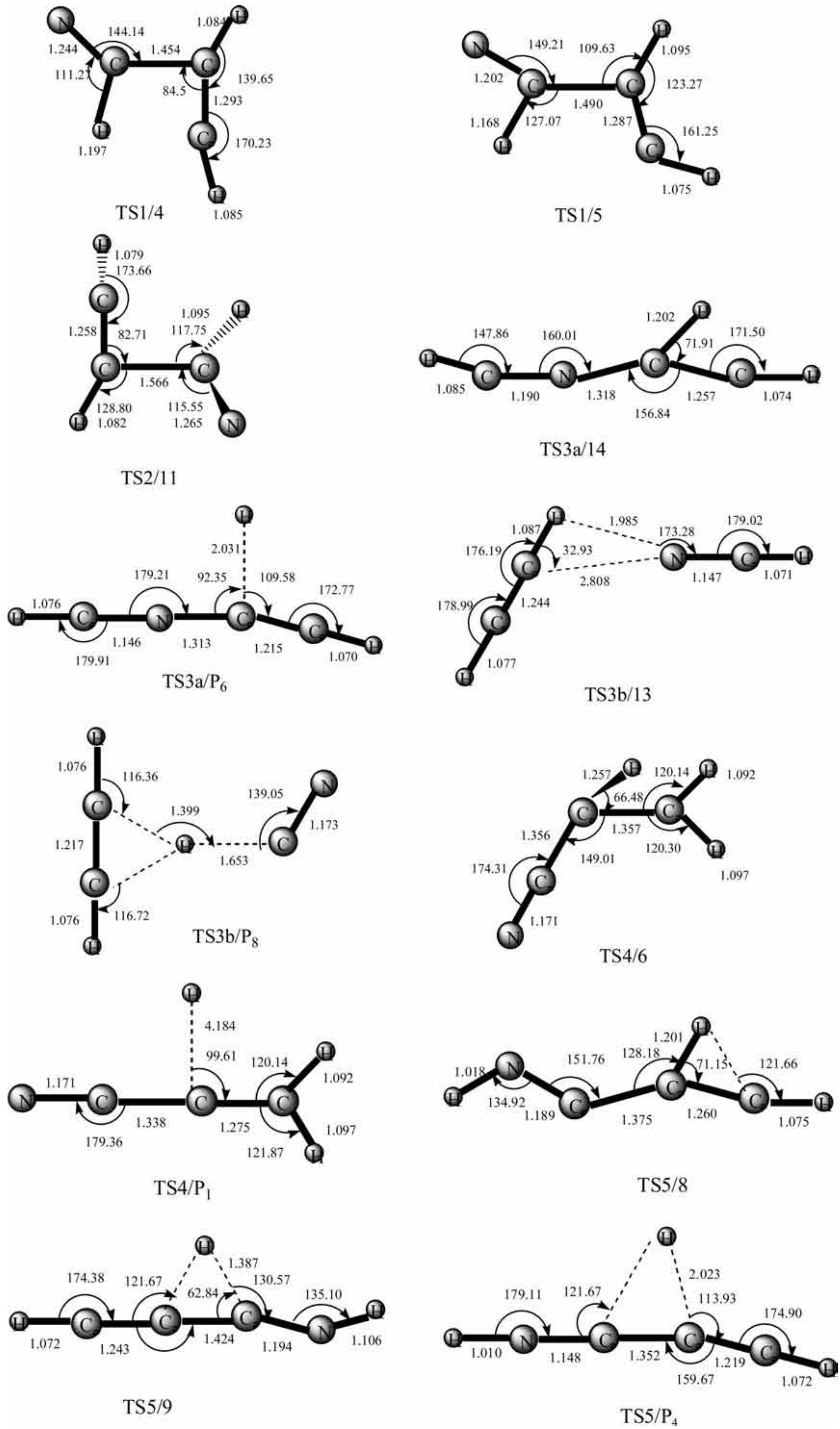
TS1/4
1.244
144.14
111.27
1.454
1.084
84.5
139.65
1.293
170.23
1.197
1.085
TS1/5
149.21
109.63
1.095
1.202
123.27
1.490
1.168
127.07
1.287
161.25
1.075
TS2/11
1.079
173.66
1.095
117.75
1.258
82.71
1.566
128.80
1.082
115.55
1.265
TS3a/14
147.86
160.01
1.202
71.91
171.50
1.085
1.190
1.318
1.257
1.074
156.84
TS3a/P_6
2.031
179.21
92.35
109.58
172.77
1.076
1.146
1.313
1.215
1.070
179.91
TS3b/13
1.087
1.985
173.28
179.02
176.19
32.93
2.808
1.147
1.071
178.99
1.244
1.077
TS3b/P_8
1.076
116.36
1.399
139.05
1.173
1.217
1.653
1.076
116.72
TS4/6
1.257
120.14
1.092
66.48
1.357
1.356
149.01
120.30
174.31
1.097
1.171
TS4/P_1
4.184
99.61
120.14
1.092
1.171
1.338
1.275
1.097
179.36
121.87
TS5/8
1.201
151.76
128.18
71.15
121.66
1.018
134.92
1.189
1.375
1.260
1.075
TS5/9
174.38
121.67
1.387
62.84
130.57
135.10
1.072
1.243
1.424
1.194
1.106
TS5/P_4
2.023
179.11
121.67
113.93
174.90
1.010
1.148
1.352
1.219
159.67
1.072

Figure 3

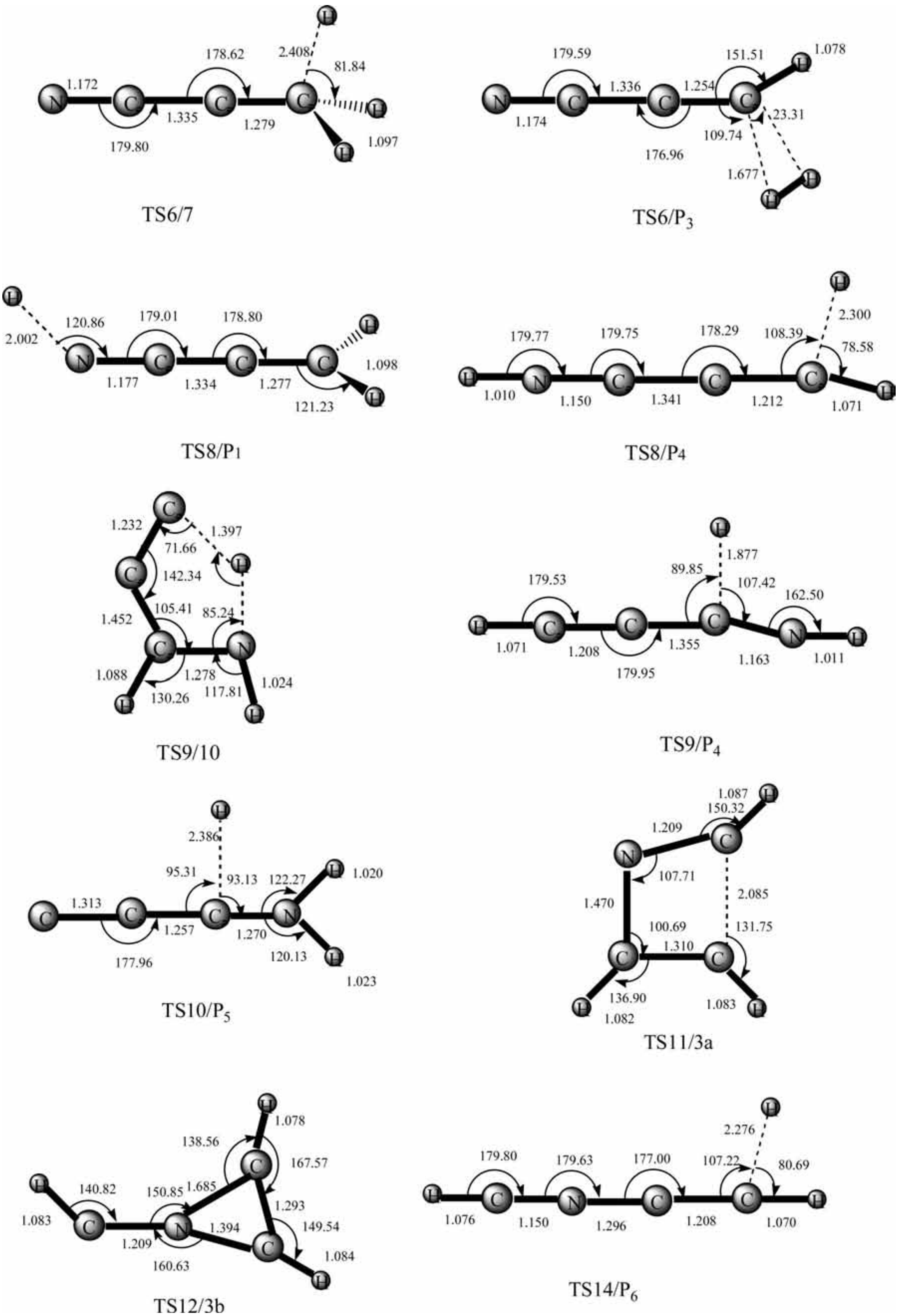

Figure 3. The optimized structures of the transition states. Distances are given in angstroms and angles in degrees.

level. So both C atom and N atom can be viewed as reactive sites. For convenient discussion, we show the reaction pathways of N-addition attacks and C-addition attacks in Figure 4, panels a and b, respectively.

3.2. Reaction Pathways. In the first place, let us discuss the formation pathways of **P$_1$**($H_2C_3N^+$+H), **P$_2$**(CN+$C_2H_3^+$), **P$_3$**(HC_3N^++H_2), **P$_4$**($HCCCNH^+$+H), and **P$_5$**(H_2NCCC^++H) which are proceeded via the C-addition intermediate **1**.

$P_1(H_2C_3N^+ + H)$

P_1($H_2C_3N^+$+H) is 32.9 kcal/mol more stable than reactant (HCN^++C_2H_2). From Figure 4a, we find that three pathways are possible.

Path P_1(1): R → 1 → 4 → P_1

Path P_1(2): R → 1 → 4 → 6 → 7 → P_1

Path P_1(3): R → 1 → 5 → 8 → P_1

1($HCCHCHN^+$) can isomerizes to **4**($NCCHCH2^+$) via the 1,3-H-shift. Then **4** either undergoes a H-elimination process to lead to **P_1** as in **path P_1(1)** or continuously isomerizes to form **6**($NCCCH_3^+$) followed by H-elimination process to generate the weakly bond complex **7**($NCCCH_2$. H^+) before the final product **P_1** as in **path P_1(2)**. It should be noted that the energy of the transition state **TS4/P_1** involved in **path P_1 (1)** lies lower in energy than **P_1** even at the higher QCISD/6-311G(d,p) calculated level. This may indicate that transition state **TS4/P_1** is kinetically unstable toward dissociation to **P_1**. Its effort in the process of **4→P_1** can be omitted. Therefore, this process can be viewed as a direct H elimination path. In **path P_1(3)**, **1** can isomerize to **5**($HCCHCNH^+$) via 1,2-H-shift from C- to N-atom. Then **5** can transform to **8**(H_2CCCNH^+) followed by its dissociation to form **P_1**.

In **path P_1(1)**, only one barrier 19.2 kcal/mol for **1→4** is needed to overcome to form **P_1**. Yet in **path P_1(2)**, three barriers

TABLE 1: Zero-Point (kcal/mol), Total (au), and Relative Energies in Parentheses (kcal/mol) As Well As Those Including Zero-Point Vibration Energies of the Reactant, Products for the HCN^++C_2H_2 Reaction

species	ZPVE		B3LYP	CCSD(T)		CCSD(T)+ZPVE
reactant	26.15167	(0.0)	−170.3099918	−169.966423	(0.0)	0.0
$P_1(H_2C_3N^+$+H)	22.07629	(−4.1)	−170.3646991	−170.012339	(−28.8)	−32.9
$P_2(CN+C_2H_3^+)$	24.77587	(−1.4)	−170.3446514	−170.000244	(−21.2)	−22.6
$P_3(HC_3N^++H_2)$	22.23738	(−3.9)	−170.3837146	−170.025678	(−37.2)	−41.1
$P_4(HCCCNH^+$+H)	23.157	(−3.0)	−170.4224455	−170.074333	(−67.7)	−70.7
$P_5(H_2NCCC^+$+H)	23.45596	(−2.7)	−170.3225859	−169.971139	(−3.0)	−5.7
$P_6(HCNCCH^+$+H)	23.49013	(−2.7)	−170.3925775	−170.044882	(−49.2)	−51.9
$P_7(C_2H_2^+$+HCN)	25.60872	(−0.5)	−170.3936551	−170.047668	(−51.0)	−51.5
$P_8(C_2H_2^+$+HNC)	26.19383	(0.0)	−170.3700264	−170.024555	(−36.5)	−36.4
$P_9(C_3N^++H_2$+H)	14.31022	(−11.8)	−170.1158316	−169.772224	(121.9)	110.0

TABLE 2: Zero-Point (kcal/mol), Total (au), and Relative Energies in Parentheses (kcal/mol) As Well As Those Including Zero-Point Vibration Energies of the Intermediates and Transition States for the HCN^++C_2H_2 Reaction

species	ZPVE		B3LYP	CCSD(T)		CCSD(T)+ZPVE
reactant	26.15167	(0.0)	−170.3099918	−169.966423	(0.0)	0.0
1	28.02003	(−1.9)	−170.4157299	−170.059968	(−58.7)	−56.8
2	27.90614	(1.8)	−170.4191187	−170.064771	(−61.7)	−60.0
3a	29.76287	(−3.6)	−170.4785473	−170.130007	(−102.6)	−99.0
3b	29.71924	(−3.6)	−170.4766139	−170.127932	(−101.3)	−97.8
4	30.66257	(−4.5)	−170.491201	−170.134313	(−105.4)	−100.8
5	29.75185	(−3.6)	−170.4986978	−170.148659	(−114.4)	−110.8
6	28.23864	(−2.1)	−170.4523107	−170.09358	(−79.8)	−77.7
7	22.63822	(−3.5)	−170.3658455	−170.012151	(−28.7)	−32.2
8	28.69308	(−2.5)	−170.5155973	−170.155289	(−118.5)	−116.0
9	28.94772	(−2.8)	−170.4657513	−170.111458	(−91.0)	−88.2
10	32.73318	(−6.6)	−170.4469692	−170.099062	(−83.2)	−76.7
11	30.7087	(4.6)	−170.4586887	−170.114235	(−92.8)	−88.2
12	29.52633	(−3.4)	−170.4224042	−170.073583	(−67.2)	−63.9
13	27.31186	(−1.2)	−170.4274237	−170.079621	(−71.0)	−69.9
14	28.70136	(−2.5)	−170.4902135	−170.128264	(−101.6)	−99.0
TS1/4	26.91255	(−0.8)	−170.3781088	−170.027509	(−38.3)	−37.6
TS1/5	25.46005	(−0.7)	−170.3906109	−170.035593	(−43.4)	−44.1
TS2/11	28.41908	(2.3)	−170.4126244	−170.064994	(−61.9)	−59.6
TS3a/14	25.04992	(−1.1)	−170.4034566	−170.044403	(−48.9)	−50.0
TS3a/P_6	24.34345	(−1.8)	−170.3860825	−170.03418	(−42.5)	−44.3
TS3b/13	27.07638	(−0.9)	−170.424425	−170.075158	(−68.2)	−67.3
TS3b/P_8	23.58486	(−2.6)	−170.3430972	−170.000755	(−21.5)	−24.1
TS4/6	27.39139	(−1.2)	−170.4334237	−170.079799	(−71.1)	−69.9
TS4/P_1	22.27127	(−3.9)	−170.3657519	−170.012845	(−29.1)	−33.0
TS5/8	25.78959	(−0.4)	−170.431954	−170.075289	(−68.3)	−68.7
TS5/9	25.66764	(−0.5)	−170.4213436	−170.057568	(−57.2)	−57.7
TS5/P_4	24.30353	(−1.8)	−170.4168192	−170.064333	(−61.4)	−63.3
TS6/7	22.6393	(−3.5)	−170.3658349	−170.011062	(−28.0)	−31.5
TS6/P_3	24.02217	(−2.1)	−170.3855246	−170.023681	(−35.9)	−38.1
TS8/P_1	23.31065	(−2.8)	−170.3634235	−170.004723	(−24.0)	−26.9
TS8/P_4	24.17206	(−2.0)	−170.4223087	−170.070381	(−65.2)	−67.2
TS9/10	27.40547	(−1.3)	−170.3353488	−169.992358	(−16.3)	−15.0
TS9/P_4	24.34611	(−1.8)	−170.4157543	−170.062585	(−60.3)	−62.1
TS10/P_5	24.21636	(−1.9)	−170.322566	−169.968304	(−1.2)	−3.1
TS11/3a	28.34201	(−2.2)	−170.4038485	−170.05665	(−56.6)	−54.4
TS12/3b	28.29195	(−2.1)	−170.4179891	−170.066923	(−63.1)	−60.9
TS14/P_6	24.0201	(−2.1)	−170.3919949	−170.041539	(−47.1)	−49.3

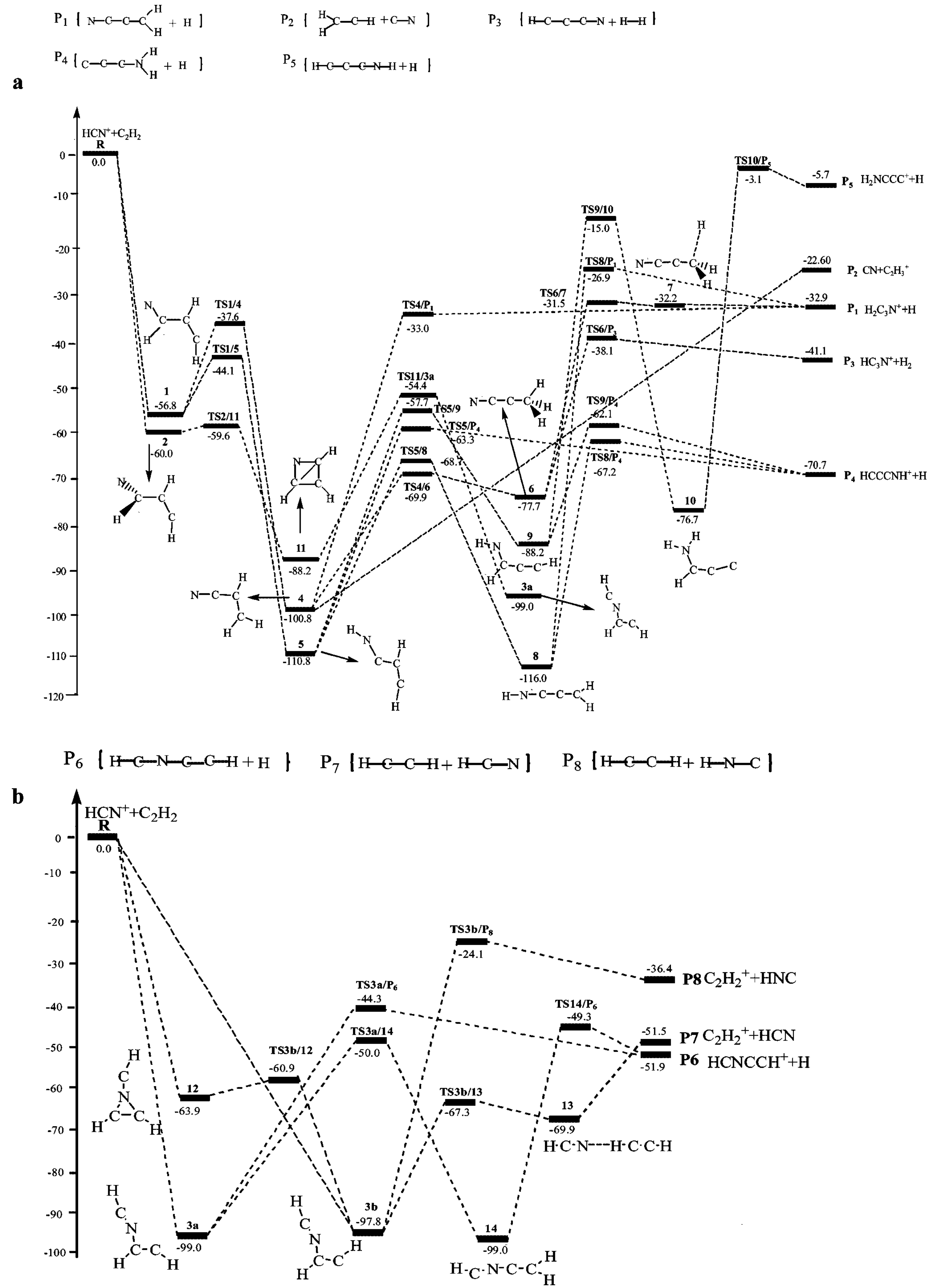

Figure 4. The sketch map of the potential energy surface (PES).

are needed, i.e., 19.2, 30.9, and 46.2 kcal/mol for **1→4**, **4→6**, and **6→7** conversions, respectively. In **path P$_1$(3)**, also three barriers have to be climbed, which are 12.7 (**1→5**), 42.1 (**5→8**), and 89.1 (**8→P$_1$**) kcal/mol. Then we expect that **path P$_1$(1)** may be the optimal channel to form **P$_1$**.

P$_2$(CN + C$_2$H$_3^+$)

We find a direct dissociation product **P$_2$**($CN+C_2H_3^+$) from **4** ($NCCHCH_2^+$), and the formation pathway of **4** has been discussed in (◆). Despite numerous attempts, we cannot locate the C−N bond rupture transition state. Therefore, we expect that this may be a single C−N bond rupture process. The formation pathway of P$_2$ can be written as

Path P$_2$: R → 1 → 4 → P$_2$

P$_3$(HC$_3$N$^+$ + H$_2$)

For product **P$_3$**($HC_3N^+ + H_2$), only one feasible pathway is located, which can be depicted as

Path P$_3$: R → 1 → 4 → 6 → P$_3$

The formation of **6**($NCCCH_3^+$) is the same as **path P$_1$(2)**. Subsequently, **6** can take H_2-elimination leading to **P$_3$**. The barrier for **6→P$_3$** conversion is 39.6kcal/mol.

P$_4$(HCCCNH$^+$ + H)

Because **P$_4$** ($HCCCNH^+ + H$) is the lowest-lying product, we find three pathways are possible

Path P$_4$(1): R → 1 → 5 → P$_4$

Path P$_4$(2): R → 1 → 5 → 8 → P$_4$

Path P$_4$(3): R → 1 → 5 → 9 → P$_4$

The formation of **5**($HCCHCNH^+$) is the same as that in **path P$_1$(3)**. **5** can either take a H-elimination process to form **P$_4$** as in **path P$_4$(1)** or continuously isomerizes to **9**($HCCCHNH^+$) followed by H-elimination process lead to **P$_4$** as in **path P$_4$(3)**. **Path P$_4$(2)** is very similar to **path P$_1$(3)**. The difference lies in the last dissociation step, i.e., in **path P$_1$(3), 8**(H_2CCCNH^+) leads to **P$_1$** via the N−H bond rupture, while in **path P$_4$(2)**, **8** gives rise to **P$_4$** via the cleavage of C−H bond.

For **path P$_4$(2)** and **path P$_4$(3)**, two barriers are needed to overcome from **5** to **P$_4$**, that is, 42.1 and 48.8 kcal/mol for **5→8** and **8→P$_4$**, respectively, as in **path P$_4$(2)**, and 53.1 and 26.1 kcal/mol for **5→9** and **9→P$_4$**, respectively, as in **path P$_4$(3)**. In **Path P$_4$(1)**, only one barrier 47.5 kcal/mol for **5→P$_4$** conversion is needed. So we expect that **path P$_4$(1)** is more competitive than **path P$_4$(2)** and **path P$_4$(3)**.

P$_5$(H$_2$NCCC$^+$ + H)

For product **P$_5$**($H_2NCCC^+ + H$), only one pathway is feasible. This path can be written as **Path P$_5$ R→1→5→9→10→P$_5$**.

The formation of **9**($HCCCHNH^+$) is the same as that in **path P$_4$(3)**. Isomer **9** requires a 1,4-H-shift to form **10**($CCCHNH_2^+$), then via a H-elimination process **10** will produce **P$_5$**. The high barrier for the steps **9→10** and **10→P$_5$** are 73.2 and 73.6 kcal/mol, respectively.

Starting from the other N-addition intermediate **2**(*v*-HCCHCHN$^+$), only one pathway is identified: ring closure to form the four-membered ring isomer **11**(c-NCHCHCH$^+$). Subsequently, **11** can isomerize to the chainlike isomer **3a**(HCNCHCH$^+$) via a ring-opening process; the evolution of **3a** will be discussed later.

SCHEME 1: Simple Frame Diagram for the Reaction $HCN^+ + C_2H_2$

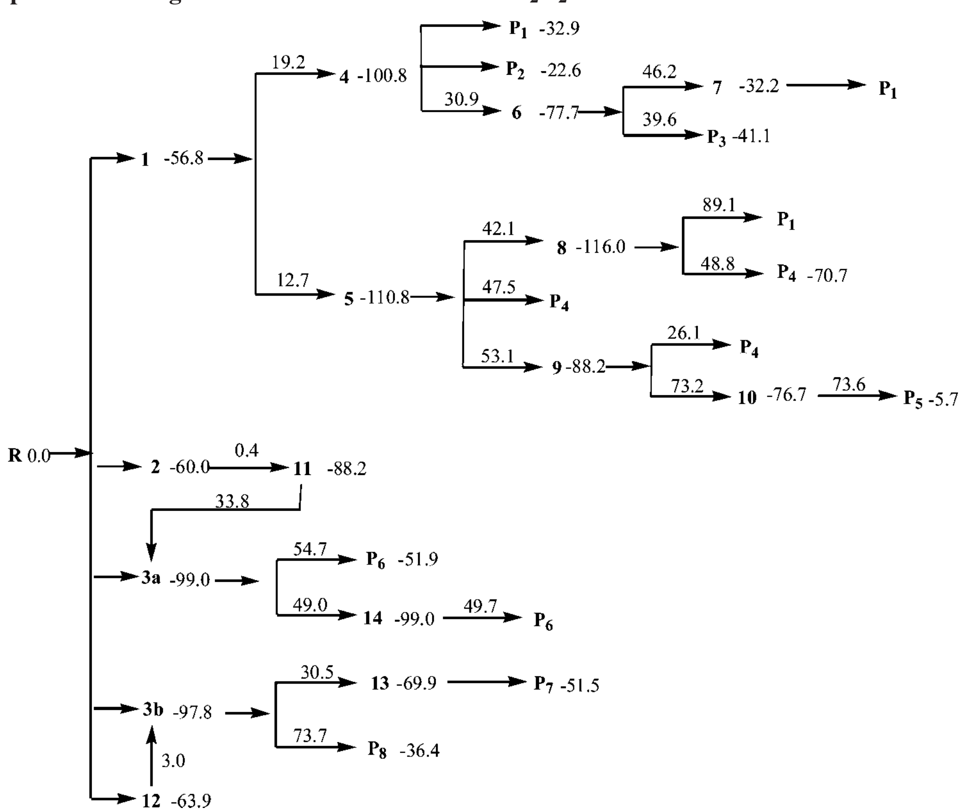

Now, we turn our attention to the formation pathways of **P$_6$**(HCNCCH$^+$+H), **P$_7$** ($C_2H_2^+$+HCN), and **P$_8$**($C_2H_2^+$+HNC). These pathways proceed via the C-addition intermediate **3**(**3a** and **3b**).

P$_6$(HCNCCH$^+$ + H)

There are two feasible pathways to form **P$_6$**(HCNCCH$^+$+H). They can be written as follows

$$\textbf{Path P}_6\textbf{(1): R} \rightarrow \textbf{3a} \rightarrow \textbf{P}_6$$

$$\textbf{Path P}_6\textbf{(2): R} \rightarrow \textbf{3a} \rightarrow \textbf{14} \rightarrow \textbf{P}_6$$

3a(HCNCHCH$^+$) can either undergo a H-elimination process that leads to **P$_6$** as in **path P$_6$(1)** or isomerizes to **14**(HCNCCH$_2^+$) via the 1,2-H-shift. Then **14** will produce **P$_6$** via H elimination. For the **3a→P$_6$** conversion, only one barrier, 54.7 kcal/mol (**3a→P$_6$**), is needed to overcome as in **path P$_6$(1)**. Yet in **path P$_6$(2)**, two barriers for **3a→14**(49.0) and **14→P$_6$**(49.7) are needed. Moreover, **path P$_6$(1)** is relatively simple, so we expect that **path P$_6$(1)** is more competitive than **path P$_6$(2)**.

P$_7$($C_2H_2^+$ + HCN)

Only one pathway is feasible to form the charge-transfer product **P$_7$**($C_2H_2^+$+HCN).

$$\textbf{Path P}_7\textbf{: R} \rightarrow \textbf{3b} \rightarrow \textbf{13} \rightarrow \textbf{P}_7$$

3b(HCNCHCH$^+$) can isomerizes to a weakly bond complex **13**(HCN···HCCH$^+$) with the barrier of 30.5 kcal/mol. Then **13** will directly dissociate to **P$_7$**.

P$_8$($C_2H_2^+$ + HNC)

3b(HCNCHCH$^+$) can directly dissociate to **P$_8$**($C_2H_2^+$+HNC) with a high barrier of 73.7 kcal/mol. The formation pathway of **P$_8$** can be written as

$$\textbf{Path P}_8\textbf{: R} \rightarrow \textbf{3b} \rightarrow \textbf{P}_8$$

4. Reaction Mechanism

In the preceding sections, we have obtained eight products, i.e., **P$_1$**($H_2C_3N^+$+H), **P$_2$**(CN+$C_2H_3^+$), **P$_3$**(HC_3N^++H_2), **P$_4$**(HCCCNH$^+$+H), **P$_5$**(H_2NCCC^++H), **P$_6$**(HCNCCH$^+$+H), **P$_7$**($C_2H_2^+$+HCN), and **P$_8$**($C_2H_2^+$+HNC). For easier discussion, the optimal channels for these eight products are listed again:

Path P$_1$(1)	**R → 1 → 4 → P$_1$**
Path P$_2$	**R → 1 → 4 → P$_2$**
Path P$_3$(1)	**R → 1 → 4 → 6 → P$_3$**
Path P$_4$(1)	**R → 1 → 5 → P$_4$**
Path P$_5$	**R → 1 → 5 → 9 → 10 → P$_5$**
Path P$_6$(1)	**R → 3a → P$_6$**
Path P$_7$	**R → 3b → 14 → P$_7$**
Path P$_8$	**R → 3b → P$_8$**

Comparing every optimal channel of forming possible products, we found that the order of energy barriers of the rate controlling step increase as follows: **Path P$_1$**(1) (19.2) = **Path P$_2$**(19.2) → **Path P$_7$**(30.5) → **Path P$_3$**(1) (39.6) → **Path P$_4$**(1) (47.5) → **Path P$_6$**(1) (54.7) → **Path P$_5$**(73.6) → **Path P$_8$**(73.7). The much higher barriers involved in the most feasible formation pathway of **P$_4$**, **P$_5$**, **P$_6$**, and **P$_8$** make these four products unlikely to be observed in experiments. As for the remaining four products, formation of **P$_1$** and **P$_2$** are kinetically the most favorable pathways. Then **P$_7$** and **P$_3$** may be kinetically the second and third feasible product. However, from Figure 4a, we can see that **P$_2$** lies 10.3 kcal/mol higher than **P$_1$**; this thermodynamically makes **P$_1$** the dominant product from **4**, and therefore **P$_2$** may have a negligible contribution to the final product. Of course, for such a complex chemical system, it is difficult to predict accurate branching ratios of various products, which need detailed dynamic or rrkm calculations. So we draw the calculation results qualitatively as a total of eight kinds of products **P$_1$**($H_2C_3N^+$+H), **P$_2$**(CN+C_2H_3+), **P$_3$**(HC_3N^++H_2), **P$_4$**(HCCCNH$^+$+H), **P$_5$**(H_2NCCC^++H), **P$_6$**(HCNCCH$^+$+H), **P$_7$**($C_2H_2^+$+HCN), and **P$_8$**($C_2H_2^+$+HNC) are kinetically feasible, the four products **P$_1$**, **P$_2$**, **P$_3$**, and **P$_7$** may be observable, while **P$_4$**, **P$_5$**, **P$_6$**, and **P$_8$** may have undetected yields. Among the four observable products, **P$_1$** is the most feasible product, **P$_7$** and **P$_3$** are the second and third products, while **P$_2$** may have only a small part.

5. Experimental Implication

In 2004, Anicich et al. performed experimental studies on the reaction HCN$^+$ + C_2H_2 using the flowing afterglow-selected ion flow tube (FA-SIFT) at room temperature. The experimental results show the products and distributions are the following: $H_2C_3N^+$ + H (0.66) > $C_2H_2^+$ + HCN (0.19) > HC_3N^+ + H_2 (0.09) > C_3N^+ + H_2+ H (0.06) > $C_2H_3^+$ + CN (0.01). Among these products, $H_2C_3N^+$ + H corresponds to **P$_1$** in our result and the distribution is the highest in all the products. $C_2H_2^+$ + HCN corresponds to **P$_7$** which also has an upper distribution. HC_3N^+ + H_2 and $C_2H_3^+$ + CN correspond to **P$_3$** and **P$_2$**, respectively. This result is in good agreement with our theoretical results. On the other hand, the experimental observed product C_3N^+ + H_2 + H may be the secondary product of **P$_3$** or **P$_1$**. However, based on our theoretical results, it is inaccessible due to the much higher relative energies 110.0 kcal/mol with respect to reactant **R**(HCN$^+$+C_2H_2). The energies of reactant, isomers, transition states, and products may be different at different temperatures, so further experimental investigation for the title reaction at higher temperatures is still desirable.

6. Conclusion

A detailed theoretical study was performed on the reaction of HCN$^+$ + C_2H_2, and the main calculated results can be summarized as follows: via the attack of the C- or N-atom of HCN$^+$ on the C_2H_2 molecule, three minimum isomers **1**(*p*-HCCHCHN$^+$), **2**(*v*-HCCHCHN$^+$), and **3**(HCNCHCH$^+$) can be formed, followed by a variety of transformations that leads to eight products. Among the eight products, **P$_1$** ($H_2C_3N^+$+H) is the most favorable product, **P$_7$** ($C_2H_2^+$+HCN) and **P$_3$** (HC_3N^++H_2) are the second and third competitive products, followed by the least feasible product **P$_2$** (CN+$C_2H_3^+$); other products, namely, **P$_4$** (HCCCNH$^+$+H), **P$_5$** (H_2NCC^++H), **P$_6$** (HCNCCH$^+$+H), and **P$_8$** ($C_2H_2^+$+HNC) may become feasible at higher temperatures. Because the intermediates and transition states involved in the reaction of HCN$^+$ + C_2H_2 are lower in energy than the reactants, the total reaction is expected to be rapid, as is confirmed by experiment. Some conclusions are in good agreement with the experimental investigations, and we hope the results may provide useful information for understanding the ion−molecule reaction in Titan's atmosphere.

Acknowledgment. This work is supported by the National Natural Science Foundation of China (No. 20773048).

References and Notes

(1) Bauer, S. J. *Adv. Space Res.* **1987**, *7*, 65.

(2) Cravens, T. E.; Robertson, I. P.; Waite, J. H.; Yelle, R. V.; Kasprzak, W. T.; Keller, C. N.; Ledvina, S. A.; Niemann, H. B.; Luhmann, J. G.; McNutt, R. L.; Ip, W. H.; DeLaHaye, V.; Mueller-Wodarg, I.; Wahlund, J. E.; Anicich, V. G.; Vuitton, V. *Geophys. Res. Lett.* **2006**, *33*, (7), Art. No. L07105.

(3) Fulchignoni, M.; Ferri, F.; Angrilli, F.; Ball, A. J.; Bar-Nun, A.; Barucci, M. A.; Bettanini, C.; Bianchini, G.; Borucki, W.; Colombatti, G.; Coradini, M.; Coustenis, A.; Debei, S.; Falkner, P.; Fanti, G.; Flamini, E.; Gaborit, V.; Grard, R.; Hamelin, M.;. M.; Harri, A.; Hathi, B.; Jernej, I.; Leese, M. R.; Lehto, A.; Lion Stoppato, P. F.; López-Moreno, J. J.; Mäkinen, T.; McDonnell, J. A. M.; McKay, C. P.; Molina-Cuberos, G.; Neubauer, F. M.; Pirronello, V.; Rodrigo, R.; Saggin, B.; Schwingenschuh, K.; Seiff, A.; Simões, F.; Svedhem, H.; Tokano, T.; Towner, M. C.; Trautner, R.; Withers, P.; Zarnecki., J. C. *Nature,* **2006**, *438*, 785.

(4) Vuitton, V.; Yelle, R. V.; McEwan, M. J. *Icarus* **2007**, *191*, 722.

(5) Broadfoot, A. L.; Sandel, B. R.; Shemansky, D. E.; Holberg, J. B.; Smith, G. R.; Strobel, D. F.; McConnell, J. C.; Kumar, S.; Hunten, D. M.; Atreya, S. K.; Donahue, T. M.; Moos, H. W.; Bertaux, J. L.; Blamont, J. E.; Pomphrey, R. B.; Linick, S. *Science* **1981**, *212*, 206.

(6) Hanel, R.; Conrath, B.; Flasar, F. M.; Kunde, V.; Maguire, W.; Pearl, J.; Pirraglia, J.; Samuelson, R.; Herath, L.; Allison, M.; Cruikshank, D.; Gautier, D.; Gierasch, P.; Horn, L.; Koppany, R.; Ponnamperuma, C. *Science* **1981**, *212*, 192.

(7) Samuelson, R.; Nath, N.; Borysow, A. *Planet. Space Sci.* **1997**, *45*, 959.

(8) Yung, Y. L.; Allen, M.; Pinto, J. P. *Appl. J. Suppl* **1984**, *55*, 465.

(9) Toublanc, D.; Parisot, J. P.; Brillet, J.; Gautier, D.; Raulin, F.; McKay, C. P. *Icarus* **1995**, *113*, 2.

(10) Ip, W. H. *Astrophys. J.* **1990**, *362*, 354.

(11) Keller, C. N.; Cravens, T. E.; Gan, L. *J. Geophys. Res.* **1992**, *97*, 12117.

(12) Xie, H. B.; Wang, J.; Zhang, S. W.; Ding, Y. H.; Sun, C. C. *J. Chem. Phys.* **2006**, *125*, 124317.

(13) Li, J. L.; Geng, C. Y.; Huang, X. R.; Zhan, J. H.; Sun, C. C. *Chem. Phys.* **2006**, *331*, 42.

(14) Yu, H. T.; Zhao, Y. L.; Kan, W.; Fu, H. G. *J. Mol. Struct.* **2006**, *772*, 45.

(15) Dong, H.; Ding, Y. H.; Sun, C. C. *J. Phys. Chem. A* **2005**, *109*, 11941.

(16) Xie, H. B.; Ding, Y. H.; Sun, C. C. *J. Phys. Chem. A* **2006**, *110*, 7262.

(17) Chen, H. T.; Ho, J. J. *J. Phys. Chem. A* **2003**, *107*, 7004.

(18) Huang, L. C. L.; Asvany, O.; Chang, A. H. H.; Balucani, N.; Lin, S. H.; Lee, Y. T.; Kaiser, R. I.; Osamura, Y. *J. Chem. Phys.* **2000**, *113*, 8656.

(19) Anicich, V. G.; Wilson, P.; McEwan, M. J. *J. Am. Soc. Mass. Spectrom.* **2004**, *15*, 1148.

(20) Milligan, D. B.; Freeman, C. G.; Maclagan, R. G. A.; McEwan, M. J.; Wilson, P. F.; Anicich, V. G. *J. Am. Soc. Mass Specrom.* **2000**, *12*, 557.

(21) Anicich, V. G.; Huntress, W. T. *Astrophys. J. Suppl. Ser.* **1986**, *62*, 553.

(22) Liu, L.; Li, Y.; Farrar, J. M. *J. Chem. Phys.* **2005**, *123*, 094304.

(23) Barrientos, C.; Largo, A. *J. Phys. Chem.* **1992**, *96*, 5808.

(24) Delrío, E.; López, R.; Menéndez, M. I.; Sordo, T. L. *J. Comput. Chem.* **1999**, *21*, 35.

(25) Qu, Z. W.; Zhu, H.; Li, Z. S.; Zhang, Q. Y. *Chem. Phys. Lett.* **2001**, *336*, 325.

(26) López, R.; Del Río, E.; Menédez, M. I.; Campomanes, P.; Sordo, T. L. *J. Mol. Struct.* **2001**, *537*, 193.

(27) Fukuzawa, K.; Matsushita, T.; Morokuma, K. J. *J. Chem. Phys.* **2001**, *115*, 3184.

(28) Chiu, Y. H.; Dressler, R. A.; Levandier, D. J.; Williams, S.; Murad, E. *J. Chem. Phys.* **1998**, *110*, 4291.

(29) Kim, H. T.; Liu, J. B.; Anderson, S. L. *J. Chem. Phys.* **2001**, *114*, 7838.

(30) Frisch, M. J.; Trucks, G. W.; Schlegel, H. B.; Scuseria, G. E.; Robb, M. A.; Cheeseman, J. R.; Zakrzewski, V. G.; Montgomery, J. A., Jr.; Stratmann, R. E.; Burant, J. C.; Dapprich, S.; Millam, J. M.; Daniels, A. D.; Kudin, K. N.; Strain, M. C.; Farkas, O.; Tomasi, J.; Barone, V.; Cossi, M.; Cammi, R.; Mennucci, B.; Pomelli, C.; Adamo, C.; Clifford, S.; Ochterski, J.; Petersson, G. A.; Ayala, P. Y.; Cui, Q.; Morokuma, K.; Malick, D. K.; Rabuck, A. D.; Raghavachari, K.; Foresman, J. B.; Cioslowski, J.; Ortiz, J. V.; Stefanov, B. B.; Liu, G.; Liashenko, A.; Piskorz, P.; Komaromi, I.; Gomperts, R.; Martin, R. L.; Fox, D. J.; Keith, T.; Al-Laham, M. A.; Peng, C. Y.; Nanayakkara, A.; Gonzalez, C.; Challacombe, M.; Gill, P. M. W.; Johnson, B. G.; Chen, W.; Wong, M. W.; Andres, J. L.; Head-Gordon, M.; Replogle, E. S.; Pople, J. A. *Gaussian 98*, revision A.6; Gaussian, Inc.: Pittsburgh, PA, 1998.

(31) Becke, A. D. *J. Chem. Phys.* **1993**, *98*, 5648.

(32) (a) Gonzalez, C.; Schlegel, H. B. *J. Chem. Phys.* **1989**, *90*, 2154. (b) Gonzalez, C.; Schlegel, H. B. *J. Chem. Phys.* **1990**, *94*, 5523.

(33) Pople, J. A.; Head-Gordon, M.; Raghavachari, K. *J. Chem. Phys.* **1987**, *87*, 5968.

JP801352Z